FOCUSING OF HIGH-BRIGHTNESS ELECTRON BEAMS WITH ACTIVE-PLASMA LENSES

R. Pompili*

Laboratori Nazionali di Frascati, Via Enrico Fermi 40, 00044 Frascati, Italy

Abstract

Plasma-based technology promises a tremendous reduction in size of accelerators used for research, medical, and industrial applications, making it possible to develop table-top machines accessible for a broader scientific community. By overcoming current limits of conventional accelerators and pushing particles to larger and larger energies, the availability of strong and tunable focusing optics is mandatory also because plasma-accelerated beams usually have large angular divergences. In this regard, active-plasma lenses represent a compact and affordable tool to generate radially symmetric magnetic fields several orders of magnitude larger than conventional quadrupoles and solenoids. However, it has been recently proved that the focusing can be highly nonlinear and induce a dramatic emittance growth. Here, we present experimental results showing how these non-linearities can be minimized and lensing improved. These achievements represent a major breakthrough toward the miniaturization of next-generation focusing devices.

INTRODUCTION

High-brightness photo-injectors are capable to drive electron beams with high peak current and low emittance as the ones required, for instance, in Plasma Wakefield Acceleration [1, 2], generation of THz [3] and FEL radiation [4], Inverse Compton Scattering [5, 6] and Transmission Electron Microscopy [7]. In such applications very dense beams are desired, thus a proper focusing system has to be considered. Permanent-magnet quadrupoles (PMQ) represent a possible approach since they reach focusing gradients up to 560 T/m [8]. However, being the focusing non-symmetric and the gradient fixed, non-trivial movable systems consisting of at least three lenses are needed in order to produce round beams with adjustable focal length. These issues can be solved by moving toward plasma-based lenses [9]. Recent results have been obtained with the so-called "active" plasma lens, demonstrating the focusing of laser-plasma accelerated electrons [10–12]. Such device consists in a discharge-capillary that generates an azimuthally symmetric magnetic field whose strength radially increases. Unlike quadrupoles, the active plasma lens focuses simultaneously in both transverse planes.

However, we have recently proved in two different works [13, 14] that such a focusing is highly nonlinear and leads to a large growth of the beam emittance. Here we report about experimental measurements demonstrating that the beam emittance can be preserved by properly shaping the beam transverse profile and by enhancing the linearity of the

---

* riccardo.pompili@lnf.infn.it

focusing field. The experiment has been performed at the SPARC_LAB test-facility [15, 16] by employing 3 cm-long discharge-capillary filled by Hydrogen gas. The characterization of the APL is done by using a 50 pC high-brightness electron beam as a probe and analyzed how the focusing influences its emittance.

EXPERIMENTAL SETUP

Figure 1 illustrates the experimental setup. The bunch is produced by the SPARC photo-injector [17], consisting in a 1.6 cell RF-gun [18] followed by two accelerating sections embedded by solenoids coils [19]. The results we report have been obtained with a 50 pC bunch at 126 MeV energy (50 keV energy spread), 1 μm normalized emittance and 1.1 ps duration, measured with a RF-Deflector device [20]. To test the APL focusing we varied the bunch transverse spot size at the capillary entrance from $\sigma_{x,y} \approx 35$ μm up to $\sigma_{x,y} \approx 160$ μm. This is the largest spot size that ensures to transport the entire beam charge (measured with a beam current monitor) across the capillary clear aperture. All quantities are quoted as rms.
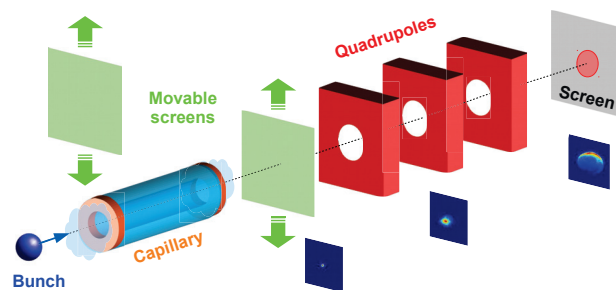
Figure 1: Experimental layout. Several screens allow to measure the beam envelope along the path. The first twos are mounted on movable actuators. Three electromagnetic quadrupoles are used to measure the beam emittance on the last screen.

The capillary consists in a sapphire hollow tube of 1 mm diameter with length $L_c = 30$ mm, filled at 1 Hz rate by H_2 gas through two symmetric inlets placed at $L_c/4$ and $3L_c/4$. The pulsed operation allows to maintain the vacuum level as low as 10^{-8} mbar in the RF linac while flowing H_2. Two electrodes, placed on each end of the capillary, are connected to a 20 kV generator producing up to 100 A peak discharge current [21]. In such conditions no pinching of the plasma is observed since it would require, for the same capillary, discharge currents of the order of few kA [22,23]. The entire apparatus is placed in a vacuum chamber directly connected with the last RF section through a windowless, three stage

differential pumping system. Since the beam encounters no windows, its emittance is not degraded due to multiple scattering. The beam envelope is measured on three consecutive Ce:YAG screens located 20, 37 and 520 cm downstream the capillary. The radiation emitted in the forward direction is then collected by a 45° mirror installed on the same screen holder. The last one is also used for emittance measurements through quadrupole scan [24, 25], using a triplet of quadrupoles installed upstream.
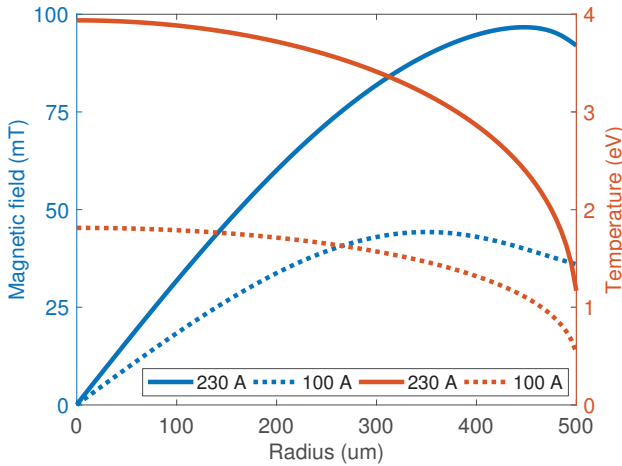
Figure 2: Calculated radial profiles of the azimuthal magnetic field (blue) and temperature (red) across the capillary. The solid (dotted) lines are obtained when plasma is produced by a 230 A (100 A) discharge current.

RESULTS

Based on the findings of our previous works we moved to a new discharge circuit able to provide currents larger than $I_D \approx 100$ A and up to $I_D \approx 230$ A. Such a current ensures that almost 90% of H_2 is ionized [26] (previously it was barely 30%) and larger temperatures reached (up to 4 eV). We show in Fig. 2 the expected radial profiles of the magnetic field and plasma temperature calculated with a one-dimensional analytical model [27]. The model computes the radial profile of plasma temperature $T(r)$ across the capillary, allowing retrieving the profile of the current density as $J(r) = \sigma_e(r)E$, with $\sigma_e \propto T(r)^{3/2}$ the electric conductivity and E the electric field associated with the discharge-current [28]. The enhanced linearity of the magnetic field, computed from the Ampere law $B_\varphi(r) = \mu_0 r^{-1} \int_0^r J(r')r'dr'$, is due to the increased plasma conductivity associated to the larger discharge-current [29].

n_b indicating the bunch density. When dealing with active plasma lenses we have therefore to consider their combined effect [14]. The nonlinearities of the overall focusing can be minimized by manipulating both the bunch shape and the capillary-discharge setup. The strength of the radial plasma wakefield is governed both by n_b and n_p [33] and its effect can be reduced by decreasing both, i.e. by operating with low plasma densities or by entering into the plasma with a large transverse spot (corresponding to a lower n_b [34]). On the contrary, the linearity of the APL field is guaranteed only at small radii since the magnetic field toward the capillary walls bends down, as shown in Fig. 2. It implies that small transverse spots are in this case preferable.
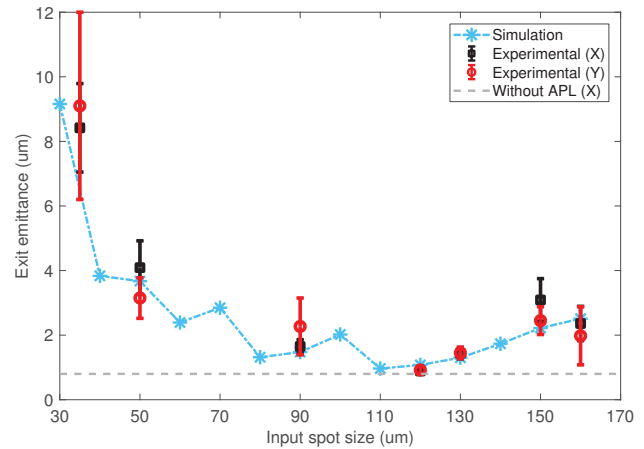
Figure 3: Resulting emittance as a function of the beam spot size at capillary entrance. The black (red) data points refer to the experimentally measured X(Y) emittances. The blue line reports the expected emittance obtained with numerical simulations. The gray line shows the unperturbed (X) beam emittance without APL.

Figure 3 shows the bunch emittance measured downstream of the capillary as a function of the spot size at its entrance. Each point is obtained for the minimum spot provided by the APL on the first screen. The tuning is achieved by delaying the discharge-current trigger with respect to the beam arrival time. For our experimental setup it corresponded to an effective current of $I_D \approx 70$ A. In the plot we have included the measured horizontal and vertical emittances and the expectations from numerical simulation (more details given later). We clearly see that for small spot sizes ($\sigma_{x,y} \approx 30\ \mu m$), there is a strong effect of the plasma wakefields due to the larger bunch density ($n_b \approx 10^{14}$ cm^{-3}). In this case the bunch emittance increases up to $\epsilon_{x,y} \approx 9\ \mu m$. Conversely, for large spot sizes ($\sigma_{x,y} \approx 160\ \mu m$, corresponding to $n_b \approx 3 \times 10^{12}$ cm^{-3}) their effect is minimized but the nonlinearities of the active lensing also increase the emittance (up to $\epsilon_{x,y} \approx 3\ \mu m$).

According to simulations of Fig. 3, the best compromise in terms of resulting emittance is obtained by entering into the plasma with a transverse spot size $\sigma_{x,y} \approx 110\ \mu m$. We thus followed this expectation and tuned the magnetic optics

In the following we discuss the plasma lens dynamics by comparing its response to different spot sizes (i.e. bunch densities). It is well known that the interaction with plasma generates beam-driven wakefields that can strongly affect the bunch dynamics [30]. In this context, passive plasma lenses have been widely investigated [31, 32] and are able produce a net beam focusing through the plasma neutralization of the space-charge fields. In our specific case we refer to the so-called *overdense* passive lenses where $n_b \ll n_p$, with

Figure 4: Bunch spot measured on the first screen downstream of the capillary with the discharge turned off (a, $\sigma_{x,y} = 105 \pm 4\ \mu m$) and on (b, $\sigma_{x,y} = 17.5 \pm 0.3\ \mu m$).

along the photo-injector to achieve an experimental spot size at capillary entrance of $\sigma_{x,y} = 115 \pm 5\ \mu m$. Figure 4(a) shows the unperturbed beam ($\sigma_{x,y} = 105 \pm 4\ \mu m$) as obtained when the discharge is turned off. Here the beam is detected on the first Ce:YAG screen downstream of the capillary (≈ 20 cm far from it). When the discharge is turned on and its delay adjusted to provide the minimum spot size on such a screen ($I_D \approx 70$ A), the beam is squeezed to $\sigma_{x,y} = 17.5 \pm 0.3\ \mu m$ as shown in Fig. 4(b) (it was $24 \pm 3\ \mu m$ with the old 100 A discharge circuit [13]). These conditions correspond also to the best results in terms of beam emittance, equal to $\epsilon_{x,y} \approx 0.9\ \mu m$. With respect to the unperturbed beam, these numbers say that such a quantity is almost preserved, at least considering the horizontal plane. The strongest focusing (and, thus, the shortest focal length) is obtained when the bunch is focused at the discharge-current peak (≈ 230 A). Here the expected waist is about $14\ \mu m$.

NUMERICAL SIMULATIONS

The study on such a beam configuration is completed by analyzing its evolution through the plasma channel with the discharge-current turned on. Considering that we are working in the overdense regime, the interaction can be described with classical 2D plasma wakefield theory in linear regime [35, 36]. The simulation also takes into account the finite plasma radial extension, being confined within the capillary radius R_c [37]. Following our previous studies in which we completely characterized the longitudinal plasma density profile along the capillary, here the channel is numerically computed by assuming a flat profile in the central part with decreasing exponential tails extending 1 cm outside the capillary [38–40]. Figure 5(a) shows a snapshot of the perturbed plasma density (Δn_p) and of the radial (W_r) and longitudinal (W_z) wakefields induced by the traveling bunch. The evolution of the beam envelope and emittance is shown in Fig. 5(b). The dotted line represents the simulated longitudinal plasma density profile. As expected there is a weak passive lens focusing in the first plasma ramp ($I_D = 0$) that also induces a slight emittance increase. Within the capillary ($I_D \neq 0$), the external discharge current increases the beam focusing and triggers an emittance oscillation that is completed in the last plasma ramp ($I_D = 0$). At the end of

the path the beam emittance is $\epsilon_{x,y} \approx 0.9\ \mu m$, in agreement with the measured one.
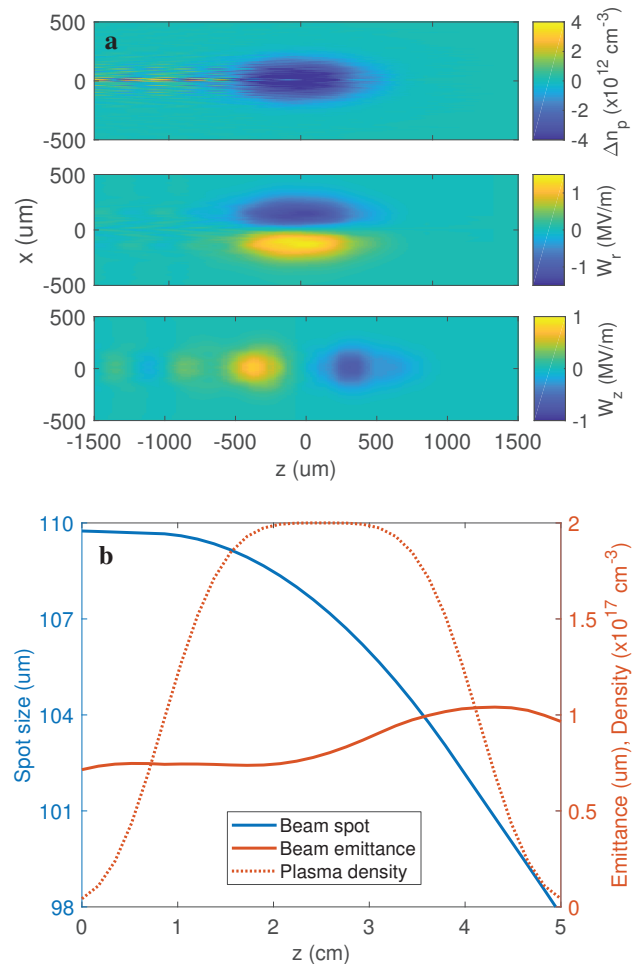
Figure 5: (a) Simulation of the perturbed plasma density (top) profile at the entrance of the plasma and computed radial (W_r, center) and longitudinal (W_z, bottom) wakefields. (b) Bunch envelope (blue) and normalized emittance (red) evolution along the plasma. The red dashed line shows the simulated plasma density profile (3 cm-long capillary with 1 cm input and exit ramps).

CONCLUSION

In conclusion, we have presented a complete characterization of an active plasma lens device consisting of a 3 cm-long capillary filled by H_2 gas. Starting from our previous works, we modified the arrangement of our experimental setup to optimize the provided lensing and preserve the beam emittance. Here we have demonstrated that by increasing the discharge-current flowing through the capillary and with a proper bunch shaping, the detrimental effects induced on the beam dynamics are minimized. Once tuned, the system allowed us to reach a stronger focusing that resulted in a beam waist of $17\ \mu m$ and minimal increase of the horizontal beam emittance ($\approx 12\%$). These results represent thus a fun-

damental step toward the development of next-generation focusing optics and demonstrate their effective usability in view of new compact facilities.

REFERENCES

[1] Pisin Chen, et al. Acceleration of electrons by the interaction of a bunched electron beam with a plasma. *Physical review letters*, 54(7):693, 1985.

[2] M Litos, et al. High-efficiency acceleration of an electron beam in a plasma wakefield accelerator. *Nature*, 515(7525):92–95, 2014.

[3] Flavio Giorgianni, et al. Strong nonlinear terahertz response induced by dirac surface states in bi2se3 topological insulator. *Nature communications*, 7, 2016.

[4] V Petrillo, et al. Observation of time-domain modulation of free-electron-laser pulses by multipeaked electron-energy spectrum. *Physical Review Letters*, 111(11):114802, 2013.

[5] Robert W Schoenlein, et al. Femtosecond x-ray pulses at 0.4 microns generated by 90 degree thomson scattering: A tool for probing the structural dynamics of materials. *Science*, 274(5285):236, 1996.

[6] A Bacci, et al. Electron linac design to drive bright compton back-scattering gamma-ray sources. *Journal of Applied Physics*, 113(19):194508–194508, 2013.

[7] R.K. Li and P Musumeci. Single-shot mev transmission electron microscopy with picosecond temporal resolution. *Physical Review Applied*, 2(2):024003, 2014.

[8] R Pompili, et al. Compact and tunable focusing device for plasma wakefield acceleration. *Review of Scientific Instruments*, 89(3):033302, 2018.

[9] Wolfgang Kurt Hermann Panofsky and WR Baker. A focusing device for the external 350-mev proton beam of the 184-inch cyclotron at berkeley. *Review of Scientific Instruments*, 21(5):445–447, 1950.

[10] J Van Tilborg, et al. Active plasma lensing for relativistic laser-plasma-accelerated electron beams. *Physical review letters*, 115(18):184802, 2015.

[11] R Pompili, et al. Focusing of high-brightness electron beams with active-plasma lenses. *Physical review letters*, 121(17):174801, 2018.

[12] CA Lindstrøm, et al. Emittance preservation in an aberration-free active plasma lens. *Physical review letters*, 121(19):194801, 2018.

[13] R Pompili, et al. Experimental characterization of active plasma lensing for electron beams. *Applied Physics Letters*, 110(10):104101, 2017.

[14] A. Marocchino, et al. Experimental characterization of the effects induced by passive plasma lens on high brightness electron bunches. *Applied Physics Letters*, 111(18):184101, 2017.

[15] M Ferrario, et al. SPARC_LAB present and future. *Nuclear Instruments and Methods B*, 309:183–188, 2013.

[16] R. Pompili, et al. Recent results at sparc-lab. *Nuclear Instruments and Methods in Physics Research Section A: Accelerators, Spectrometers, Detectors and Associated Equipment*, 2018.

[17] D Alesini, et al. The sparc project: a high-brightness electron beam source at lnf to drive a sase-fel experiment. *Nuclear Instruments and Methods A*, 507(1–2):345 – 349, 2003.

[18] A Cianchi, et al. High brightness electron beam emittance evolution measurements in an rf photoinjector. *Physical Review Special Topics-Accelerators and Beams*, 11(3):032801, 2008.

[19] M Ferrario, et al. Experimental demonstration of emittance compensation with velocity bunching. *Physical review letters*, 104(5):054801, 2010.

[20] David Alesini, et al. Rf deflector design and measurements for the longitudinal and transverse phase space characterization at sparc. *Nuclear Instruments and Methods in Physics Research Section A: Accelerators, Spectrometers, Detectors and Associated Equipment*, 568(2):488–502, 2006.

[21] MP Anania, et al. Plasma production for electron acceleration by resonant plasma wave. *Nuclear Instruments and Methods in Physics Research Section A: Accelerators, Spectrometers, Detectors and Associated Equipment*, 2016.

[22] NA Bobrova, et al. Mhd simulations of plasma dynamics in pinch discharges in capillary plasmas. *Laser and particle beams*, 18(04):623–638, 2000.

[23] DJ Spence, et al. Gas-filled capillary discharge waveguides. *JOSA B*, 20(1):138–151, 2003.

[24] Andrea Mostacci, et al. Chromatic effects in quadrupole scan emittance measurements. *Physical Review Special Topics-Accelerators and Beams*, 15(8):082802, 2012.

[25] A Cianchi, et al. Six-dimensional measurements of trains of high brightness electron bunches. *Physical Review Special Topics-Accelerators and Beams*, 18(8):082804, 2015.

[26] E Brentegani, et al. Numerical studies on capillary discharges as focusing elements for electron beams. *Nuclear Instruments and Methods in Physics Research Section A: Accelerators, Spectrometers, Detectors and Associated Equipment*, 2018.

[27] NA Bobrova, et al. Simulations of a hydrogen-filled capillary discharge waveguide. *Physical Review E*, 65(1):016407, 2001.

[28] Shalom Eliezer. *The interaction of high-power lasers with plasmas*. CRC Press, 2002.

[29] Gennadiy Bagdasarov, et al. Plasma equilibrium inside various cross-section capillary discharges. *Physics of Plasmas*, 24(5):053111, 2017.

[30] R Govil, et al. Observation of return current effects in a passive plasma lens. *Physical review letters*, 83(16):3202, 1999.

[31] JJ Su, et al. Plasma lenses for focusing particle beams. *Physical Review A*, 41(6):3321, 1990.

[32] G Hairapetian, et al. Experimental demonstration of dynamic focusing of a relativistic electron bunch by an overdense plasma lens. *Physical review letters*, 72(15):2403, 1994.

[33] Pisin Chen, et al. Plasma focusing for high-energy beams. *IEEE transactions on plasma science*, 15(2):218–225, 1987.

[34] J Van Tilborg, et al. Comparative study of active plasma lenses in high-quality electron accelerator transport lines. *Physics of Plasmas*, 25(5):056702, 2018.

[35] W Lu, et al. Limits of linear plasma wakefield theory for electron or positron beams. *Physics of Plasmas*, 12(6):063101, 2005.

[36] A Marocchino, et al. Efficient modeling of plasma wakefield acceleration in quasi-non-linear-regimes with the hybrid code architect. *Nuclear Instruments and Methods in Physics Research Section A: Accelerators, Spectrometers, Detectors and Associated Equipment*, 829:386–391, 2016.

[37] Y Fang, et al. The effect of plasma radius and profile on the development of self-modulation instability of electron bunches. *Physics of Plasmas*, 21(5):056703, 2014.

[38] F Filippi, et al. Spectroscopic measurements of plasma emission light for plasma-based acceleration experiments. *Journal of Instrumentation*, 11(09):C09015, 2016.

[39] A Biagioni, et al. Electron density measurement in gas discharge plasmas by optical and acoustic methods. *Journal of Instrumentation*, 11(08):C08003, 2016.

[40] F Filippi, et al. Tapering of plasma density ramp profiles for adiabatic lens experiments. *Nuclear Instruments and Methods in Physics Research Section A: Accelerators, Spectrometers, Detectors and Associated Equipment*, 2018.

MC3: Novel Particle Sources and Acceleration Techniques

A16 Advanced Concepts